

# Diffuse Source Absolute Sensitivity and Point Source Relative Sensitivity as a Function of Extraction Slit Height for STIS First-Order Modes

---

Ralph Bohlin, Space Telescope Science Institute  
1998 February

---

## ABSTRACT

*Sensitivities for point sources relative to the standard 11 or 7 pixel height are presented for a selection of other extraction heights. Typical uncertainties in these relative throughputs are less than 1–2%.*

*The diffuse source, specific intensity calibration is defined in terms of the infinite extraction height for point sources.*

---

## 1. Introduction

The absolute flux calibration for point source spectra in the low dispersion modes (Bohlin, Collins, & Gonnella 1998) is for an extraction height of 11 px for the MAMA modes and 7 px for the CCD spectra (Leitherer & Bohlin 1997) and is used in computing the flux values in the \*.SX1 STIS calibrated data files. The extraction height is included in the data header. Extractions of different heights are required for considerations of signal-to-noise (S/N), purity in spectral lines, and diffuse source sensitivity calibration in the \*.SX2 files. Therefore, the response,  $H(h)$ , for nine different extraction heights,  $h$ , are computed relative to the standard size of 11 or 7 px. Eight of these heights are 3, 5, 7, 9, 11, 15, 21, and 600 px, while the ninth height depends on the mode per Table 1. These data files can be found in the STScI Calibration Data Base with the names \*pct.fits and are documented in ICD-47. See the Data Handbook for a detailed description of pipeline output products.

**Table 1.** Ninth Extraction Height in Pixels

Mode	G140L	G230L	G230LB	G430L	G750L
Height	140	110	80	64	200

## 2. Observations, Analysis, and Results

### *Low dispersion*

Leitherer & Bohlin (1997) show the STIS PSF perpendicular to the dispersion. Because of the STIS plate scale with a high magnification, the wings of the PSF extend over hundreds of pixels. Each STIS entrance aperture truncates the PSF from the OTA differently, so that the distribution of light perpendicular to the dispersion, H, is different for each entrance slit. On the other hand, one high S/N spectrum suffices to define H(h), the relative throughput as a function of extraction height, h. The set of observations currently available and adequate for defining H for a particular mode and slit are in Table 2.

**Table 2.** Observations

ROOTNAME	MODE	CEN-WAVE	APER	TARGET	DATE	PROP-ID (sec)	EXP-TIME
O3YX14HSM	G140L	1425	52X2	GRW+70D5824	21/06/97	7064	240.0
O3YX15QEM	G140L	1425	52X2	GRW+70D5824	29/06/97	7064	240.0
O3YX16KLM	G140L	1425	52X2	GRW+70D5824	05/07/97	7064	240.0
O45901010	G140L	1425	52X2	GRW+70D5824	12/08/97	7673	180.0
O45910010	G140L	1425	52X2	GRW+70D5824	16/09/97	7673	180.0
O45911010	G140L	1425	52X2	GRW+70D5824	06/10/97	7673	180.0
O45912010	G140L	1425	52X2	GRW+70D5824	17/11/97	7673	180.0
O43J01QAM	G140L	1425	52X2	GD153	09/07/97	7097	60.0
O3ZX08HHM	G140L	1425	52X2	GD153	13/07/97	7096	187.1
O48X01070	G140L	1425	52X2	GRW+70D5824	31/10/97	7721	60.0
O4DD06020	G140L	1425	25MAMA	GD71	30/11/97	7657	120.0
O48X01010	G140L	1425	0.2X0.06	GRW+70D5824	31/10/97	7721	300.0
O48X01020	G140L	1425	0.2X0.09	GRW+70D5824	31/10/97	7721	200.0
O48X01030	G140L	1425	52X0.05	GRW+70D5824	31/10/97	7721	250.0
O48X01040	G140L	1425	52X0.1	GRW+70D5824	31/10/97	7721	150.0
O48X01050	G140L	1425	52X0.2	GRW+70D5824	31/10/97	7721	100.0
O48X01060	G140L	1425	52X0.5	GRW+70D5824	31/10/97	7721	100.0

**Table 2.** Observations (Continued)

ROOTNAME	MODE	CEN-WAVE	APER	TARGET	DATE	PROP-ID (sec)	EXP-TIME
O3YX11P2M	G230L	2376	52X2	GRW+70D5824	29/05/97	7064	636.0
O3YX12UTM	G230L	2376	52X2	GRW+70D5824	06/06/97	7064	636.0
O3YX13TQM	G230L	2376	52X2	GRW+70D5824	13/06/97	7064	636.0
O3YX14HWM	G230L	2376	52X2	GRW+70D5824	21/06/97	7064	636.0
O3YX15QIM	G230L	2376	52X2	GRW+70D5824	29/06/97	7064	636.0
O3YX16KPM	G230L	2376	52X2	GRW+70D5824	05/07/97	7064	636.0
O45901020	G230L	2376	52X2	GRW+70D5824	12/08/97	7673	184.0
O45910020	G230L	2376	52X2	GRW+70D5824	16/09/97	7673	184.0
O45911020	G230L	2376	52X2	GRW+70D5824	06/10/97	7673	184.0
O45912020	G230L	2376	52X2	GRW+70D5824	17/11/97	7673	184.0
O3ZX08HLM	G230L	2376	52X2	GD153	13/07/97	7096	187.1
O40901NSM	G230L	2376	52X2	HZ21	28/05/97	7101	360.0
O48X010E0	G230L	2376	52X2	GRW+70D5824	31/10/97	7721	150.0
O4DD07020	G230L	2376	25MAMA	GD71	30/11/97	7657	120.0
O48X01080	G230L	2376	0.2X0.06	GRW+70D5824	31/10/97	7721	350.0
O48X01090	G230L	2376	0.2X0.09	GRW+70D5824	31/10/97	7721	300.0
O48X010A0	G230L	2376	52X0.05	GRW+70D5824	31/10/97	7721	350.0
O48X010B0	G230L	2376	52X0.1	GRW+70D5824	31/10/97	7721	150.0
O48X010C0	G230L	2376	52X0.2	GRW+70D5824	31/10/97	7721	150.0
O48X010D0	G230L	2376	52X0.5	GRW+70D5824	31/10/97	7721	150.0
O3WY02010	G230LB	2375	52X2	BD+75D325	18/05/97	7094	162.0
O3TT42010	G230LB	2375	52X2	GD153	21/05/97	7063	600.0
O3TT43010	G230LB	2375	52X2	GD153	28/05/97	7063	600.0
O3TT44010	G230LB	2375	52X2	GD153	04/06/97	7063	600.0
O3TT45010	G230LB	2375	52X2	GD153	10/06/97	7063	600.0
O3TT46010	G230LB	2375	52X2	GD153	18/06/97	7063	600.0
O3TT47010	G230LB	2375	52X2	GD153	25/06/97	7063	600.0
O3TT48010	G230LB	2375	52X2	GD153	01/07/97	7063	600.0
O3WY02030	G430L	4300	52X2	BD+75D325	18/05/97	7094	122.4
O3TT42020	G430L	4300	52X2	GD153	21/05/97	7063	252.0
O3TT43020	G430L	4300	52X2	GD153	28/05/97	7063	252.0

**Table 2.** Observations (Continued)

ROOTNAME	MODE	CEN-WAVE	APER	TARGET	DATE	PROP-ID (sec)	EXP-TIME
O3TT44020	G430L	4300	52X2	GD153	04/06/97	7063	252.0
O3TT45020	G430L	4300	52X2	GD153	10/06/97	7063	252.0
O3TT46020	G430L	4300	52X2	GD153	18/06/97	7063	252.0
O3TT47020	G430L	4300	52X2	GD153	25/06/97	7063	252.0
O3TT48020	G430L	4300	52X2	GD153	01/07/97	7063	252.0
O40801010	G430L	4300	52X2	FEIGE110	13/06/97	7100	72.0
O40801090	G430L	4300	52X0.05	FEIGE110	13/06/97	7100	192.0
O40801070	G430L	4300	52X0.1	FEIGE110	13/06/97	7100	120.0
O40801050	G430L	4300	52X0.2	FEIGE110	13/06/97	7100	72.0
O40801030	G430L	4300	52X0.5	FEIGE110	13/06/97	7100	72.0
O3WY02040	G750L	7751	52X2	BD+75D325	18/05/97	7094	199.0
O3TT42040	G750L	7751	52X2	GD153	21/05/97	7063	3240.0
O3TT43040	G750L	7751	52X2	GD153	28/05/97	7063	3240.0
O3TT44040	G750L	7751	52X2	GD153	04/06/97	7063	3240.0
O3TT45040	G750L	7751	52X2	GD153	10/06/97	7063	3240.0
O3TT46040	G750L	7751	52X2	GD153	18/06/97	7063	2282.0
O3TT47040	G750L	7751	52X2	GD153	25/06/97	7063	2282.0
O3TT48040	G750L	7751	52X2	GD153	01/07/97	7063	2282.0
O40801020	G750L	7751	52X2	FEIGE110	13/06/97	7100	120.0
O408010A0	G750L	7751	52X0.05	FEIGE110	13/06/97	7100	240.0
O40801080	G750L	7751	52X0.1	FEIGE110	13/06/97	7100	168.0
O40801060	G750L	7751	52X0.2	FEIGE110	13/06/97	7100	120.0
O40801040	G750L	7751	52X0.5	FEIGE110	13/06/97	7100	120.0
O3ZX09E3M	G140M	1173	52X2	GD153	26/05/97	7096	2236.0
O3ZX09EFM	G140M	1420	52X2	GD153	27/05/97	7096	552.0
O3ZX09E7M	G140M	1616	52X2	GD153	27/05/97	7096	2600.0
O43J02GLM	G140M	1272	52X2	GD153	13/07/97	7097	156.0
O43J03Z7M	G140M	1518	52X2	GD153	25/07/97	7097	500.0
O3ZX09EBM	G230M	1687	52X2	GD153	27/05/97	7096	2500.0
O3ZX09EJM	G230M	2338	52X2	GD153	27/05/97	7096	975.0
O3ZX09ENM	G230M	2977	52X2	GD153	27/05/97	7096	2705.0

**Table 2.** Observations (Continued)

ROOTNAME	MODE	CEN-WAVE	APER	TARGET	DATE	PROP-ID (sec)	EXP-TIME
O43J04EEM	G230M	1851	52X2	GD153	21/07/97	7097	550.0
O43J05EUM	G230M	2659	52X2	GD153	19/07/97	7097	585.6
o3wy02060	G230MB	1713	52X2	BD+75D325	18/05/97	7094	170.0
o3wy02070	G230MB	2276	52X2	BD+75D325	18/05/97	7094	120.0
o3wy02080	G230MB	3115	52X2	BD+75D325	18/05/97	7094	120.0
o3wy02090	G430M	3165	52X2	BD+75D325	18/05/97	7094	126.0
o3wy020a0	G430M	4451	52X2	BD+75D325	18/05/97	7094	132.0
o3wy020b0	G430M	4451	52X2	BD+75D325	18/05/97	7094	120.0
O3wy020c0	G430M	4451	52X2	BD+75D325	18/05/97	7094	120.0
o3wy020e0	G430M	5471	52X2	BD+75D325	18/05/97	7094	120.0
o3wy020f0	G750M	5734	52X2	BD+75D325	18/05/97	7094	129.0
o3wy020g0	G750M	7795	52X2	BD+75D325	18/05/97	7094	144.0
o3wy020h0	G750M	10363	52X2	BD+75D325	18/05/97	7094	588.0

For the narrow slit observations with the MAMA detectors in proposal 7101, the target is not in the slit. Additional CCD observations from 7721 are short exposures and do not improve the CCD results from 7100.

Each spectral image in Table 2 is extracted with standard CALSTIS processing for each of the 9 heights to produce 9 spectra. The background is measured at 300 px above and below the spectrum with an extraction height of 11 px and is median filtered with a width of 9 px. Except for G140L, which is contaminated by the geocoronal emission at Ly- $\alpha$ , the filtered background is fit with a third order polynomial to get a smooth background estimate. To produce the H(h) functions, these spectra are normalized by dividing by the spectrum for the standard height, h=11 px for the MAMA's and 7 px for the CCD modes. Splines with 12 equally spaced nodes are fit to the normalized H functions.

Figure 1 is an example of the derived H functions and the spline fits. The data deviate from the smooth fits at the shortest wavelengths and in the region of the strong Ly- $\alpha$  line because of impure light from the wings of the PSF that add light of the wrong wavelength to the pure spectrum. The amount of the contaminating light is reduced for shorter extraction heights, h, which is demonstrated by the dip below the fits at Ly- $\alpha$  for h less than the standard 11px and by the blip above the fits for h>11. By ignoring the impure light, the spline fits leave the contamination unchanged when used to compute the absolute flux per ISR 97-14 (Bohlin, Collins, & Gonnella 1998). In other words, absolute fluxes are NOT reliable near the sharp sensitivity cutoff below  $\sim 1150\text{\AA}$  or in the cores of strong lines at the

10–20% level for the 52x2 slit. If a correction algorithm is ever developed for this out-of-band contamination, then the expectation is that the systematic deviations from the smooth fits would vanish for fits to a corrected spectrum. The amount of contamination illustrated at Ly- $\alpha$  approaches a worst case, except where the PSF blooms longward of  $\sim 8000\text{\AA}$  due to scattering within the CCD substrate. STIS spectra are more pure than illustrated in Figure 1 for narrower slits than the 52x2 and for longer wavelengths where the OTA PSF shrinks.

Figures 2-3 show measured H functions and the spline fits for a small 0.2x0.06 arcsec slit for G140L and G230L, respectively. The smaller slit demonstrates a more compact signal distribution perpendicular to the dispersion with only  $\sim 3\%$  more flux in the  $h=600$  extraction vs.  $h=11$  at  $1400\text{\AA}$  in Figure 2, while the 52x2 slit in Figure 1 has a corresponding increase of 38%. An  $h=3$  extraction has a larger fraction of the total signal in Figure 2 vs. Figure 1. For G230L in Figure 3, the PSF is comparable to the G140L PSF at the longer wavelengths in Figure 2 with the same entrance slit. The artifacts that are evident in the data for  $h=3$  in Figure 3 are a quantitative example of the poor photometry associated with such limited extractions, although  $h=3$  might provide the purest absorption line profile.

Figures 4-8 are the derived  $H(h)$  results for the five low dispersion modes and the 52x2 arcsec slit, which has multiple observations. The bars at each spline node are the  $1-\sigma$  scatter among the values of the spline fits. In general, only the  $h=3$  extraction height is photometrically poor with error bars greatly exceeding the size of the plotted symbols. A dashed line connects the largest  $h=600$  extraction. The second largest extraction height (dotted line) contains  $\sim 99\%$  of the signal and is often a more robust estimate of the total signal than the  $h=600$  extraction, which contains  $\sim 60\%$  of the image and 60% of the total background noise. For example, the G230LB point at  $1775\text{\AA}$  shows a few percent scatter for  $h=600$ , while the  $h=80$  extraction has all but a few percent of the signal and an uncertainty of less than 1%. Similarly, the G750L extraction for  $h=200$  is better defined than the  $h=600$  value at  $9850\text{\AA}$ .

Figures 9–30 show  $H(h)$  for commonly used entrance apertures, corresponding to the low dispersion entries in Table 2. These Figures cover the range of slit widths and lengths, so that the relative throughput, H, for a particular extraction height, h, can be estimated for entrance slits that are not measured. For example, the missing small slits for G230LB could be estimated by correcting H for the slit of interest for G430L, by the ratio of the curves for G230LB to G430L for the 52x2 slit. The accuracy of this process could be estimated by repeating the procedure for the same small slit and G750L to see how close the estimate is to the actual measurement for G750L. Figures 9 and 16 for the wide open 25MAMA aperture are identical within uncertainties to the results for the 52x2 slit, except for a few percent higher values of H for the largest two extraction heights h. For G230L and the standard extraction of  $h=11$ , slits of 0.2 arcsec and narrower contain all but a few

percent of the total stellar signal, while the same is true for G430L and the standard  $h=7$  for slits of 0.5 arcsec and narrower. For G750L, the 52x0.2 slit, and the longest wavelengths, the  $h=600$  fit is spuriously following noise, while the  $h=200$  curve is a better indication of the total signal relative to the standard  $h=7$ .

### ***Medium Dispersion***

Overplotted as triangles, Figures 4-8 also show sample results for the 52x2 entrance slit and the *medium* dispersion first order gratings. In general, the medium dispersion  $H(h)$  functions are in agreement with the low dispersion results within uncertainties. Exceptions include the shortest wavelengths of G140M, which have a more extended PSF than the G140L. However, the actual G140L data in Figures 1-2 are more extended than the spline fits in Figure 4, because the point where impure light begins to dominates is obvious and abrupt between 1150-1160Å and can be easily ignored in the spline fits. In the medium dispersion, the width of the PSF in Ångstroms is less and the impure light contamination is more insidious, which causes the gradually increasing deviation of the medium dispersion triangles from the low dispersion fits from 1200Å toward shorter wavelengths.

Other deviations of the medium dispersion data from the low dispersion fits are caused by noise for large extraction heights  $h$  and by residual geometric distortions for small  $h$  values at the edges of the detector, which emphasizes again the poorer photometric precision for the largest and smallest  $h$  values. The more compact PSF for G750M-7795 might be due to the lack of any light on the detector at the longest wavelengths, where the CCD scattering is the worst. More data and analysis are needed to define a precise set of  $H$  functions for medium dispersion.

## **3. Extended Source Calibration**

The absolute energy for diffuse objects is in units of flux per unit surface area, usually referred to as specific intensity with symbol  $I$ . The specific intensity calibration for a continuum source of infinite extent , i.e. large with respect to the few arcsec extent of the far wings of the STIS psf, is:

$$I(\text{contin}) = R \cdot T(52x2) / [S \cdot H_{\max}(52x2) \cdot \Omega(\text{slit})]$$

(Bohlin, Lindler, & Baum 1996) where:  $R$  is the flat fielded countrate in a pixel.  $S$  is the point source sensitivity for the  $h=11$  or  $7$  extraction height and the 52x2 arcsec entrance slit.  $\Omega(\text{slit})$  is the solid angle in square arcsec subtended by the pixel height (i.e., plate scale perpendicular to the dispersion) times the slit width  $W$ .  $T(52x2)$  is the transmission of the 52x2 arcsec slit as a function of wavelength (relative to  $T(\text{clear})=1$ .)

$H_{\max}(52x2)$  is the new photometric correction of order unity that is plotted as a function of wavelength in Figures 4-8 for extraction slit height  $h=600$  px.  $T(52x2)/H_{\max}$  is not included in (Bohlin, Lindler, & Baum 1996), because the extended nature of the PSF was

not anticipated. Hmax is the ratio of signal in an infinite (600px) high spectral extraction slit to the standard 11px for the MAMA's and 7px for the CCD. A 52x2 slit with a 2 arcsec width captures all but a few percent of the total point source PSF. The correction factor of T/Hmax arises, because the light lost in the wings of the PSF for the part of the sky INSIDE the slit comes back to the pixel of interest in the wings of the PSF for regions of sky OUTSIDE the entrance slit for an infinitely extended diffuse source. Therefore, corrections must be made to 52x2 point source calibration for the light lost from the h=7 or 11 px extraction height, i.e. Hmax(52x2), and for the small bit of light lost outside the 2 arcsec width, i.e., T(52x2).

The corresponding calibration for a diffuse emission line object is

$$I(\text{line}) = R \cdot d \cdot T(52x2) / [S \cdot Hmax(52x2) \cdot \Omega(\text{px})]$$

where  $d$  is the dispersion in  $\text{\AA}/\text{px}$ .  $\Omega(\text{px})$  is the area in square arcsec of one pixel for slits wider than a one pixel width.

The extraction of a STIS spectrum with  $h=600$  to get all of the flux of a point source is subject to noise from 60% of the image, which can cause poor spline fits, especially for the CCD. Therefore, a much smaller  $h$  value is selected for each mode per Table 1 to extract about 99% of the total signal. This 8th extraction height provides a check on the accuracy of the  $h=600$  case, as well as an alternative choice for computing the diffuse source calibration. The outstanding example of a bad fit for  $h=600$  is in Figure 29, where the long wavelength fit for  $h=600$  drops below the splines for  $h=200$ . By comparison with Figures 8, 28, and 30, the correct value for  $h=600$  around 10,000 $\text{\AA}$  can be estimated.

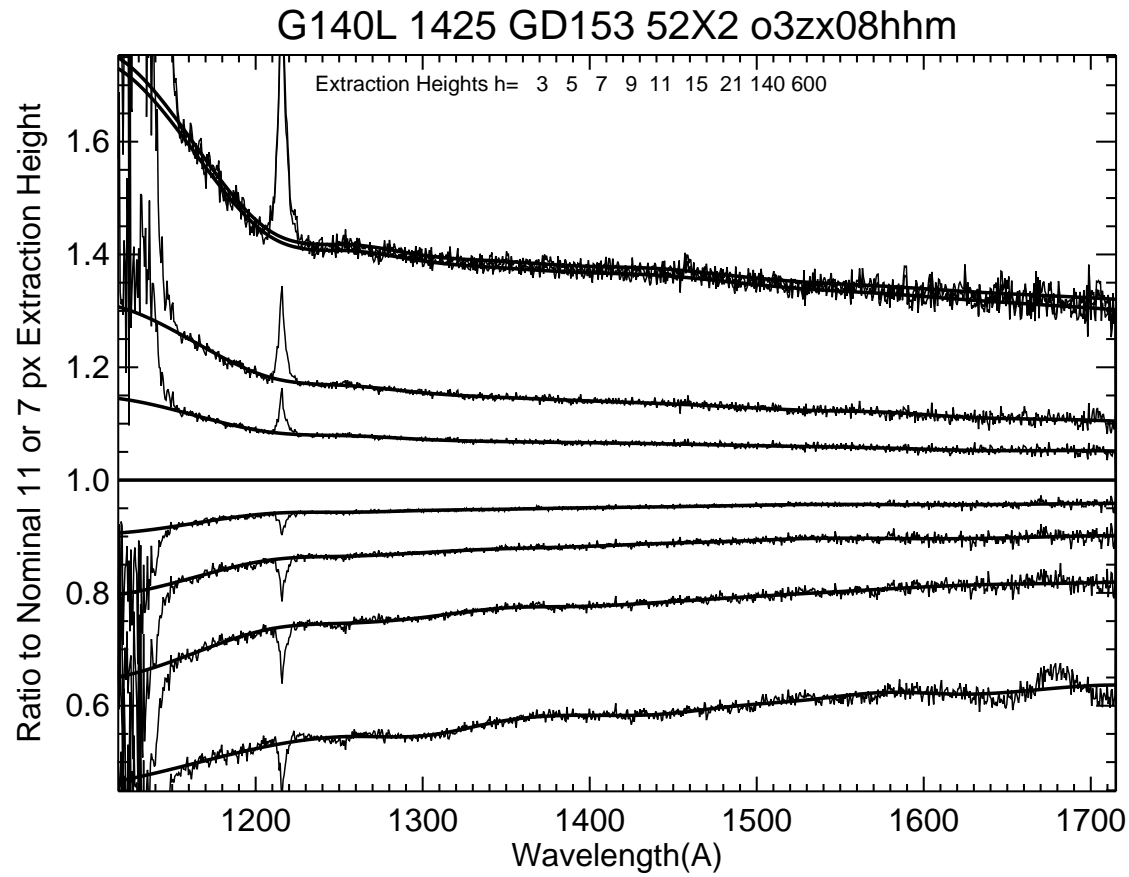
## 4. Acknowledgements

Thanks to Don Lindler for advice, suggestions, and software support.

## 5. References

- Bohlin, R., Collins, N., & Gonnella, A. 1998, Instrument Science Report, STIS 97-14, (Baltimore:STScI).
- Bohlin, R., Lindler, D., & Baum S. 1996, Instrument Science Report, STIS 96-015, (Baltimore:STScI).
- Leitherer, C. & Bohlin, R. 1997, Instrument Science Report, STIS 97-13, (Baltimore:STScI).

**Figure 1:** Ratios to the standard  $h=11$  for G140L spectra obtained in the  $52 \times 2$  arcsec slit and extracted with the extraction heights,  $h$ , indicated at the top of the plot. The smooth solid lines are the spline fits to the data with 12 equally spaced nodes and the nine values of  $h$  increasing for the nine curves from bottom to top. The 5th curve from the bottom for  $h=11$  is unity. The 8th and 9th curves at the top for  $h=140$  and  $600\text{px}$  are nearly coincident. The shortest wavelengths and the region around Ly- $\alpha$  are contaminated by spectrally impure light and are ignored in fitting the splines.



BOHLIN: abscor 12-Jan-1998 16:10

**Figure 2:** As in Figure 1, except for the 0.2x0.06 slit.

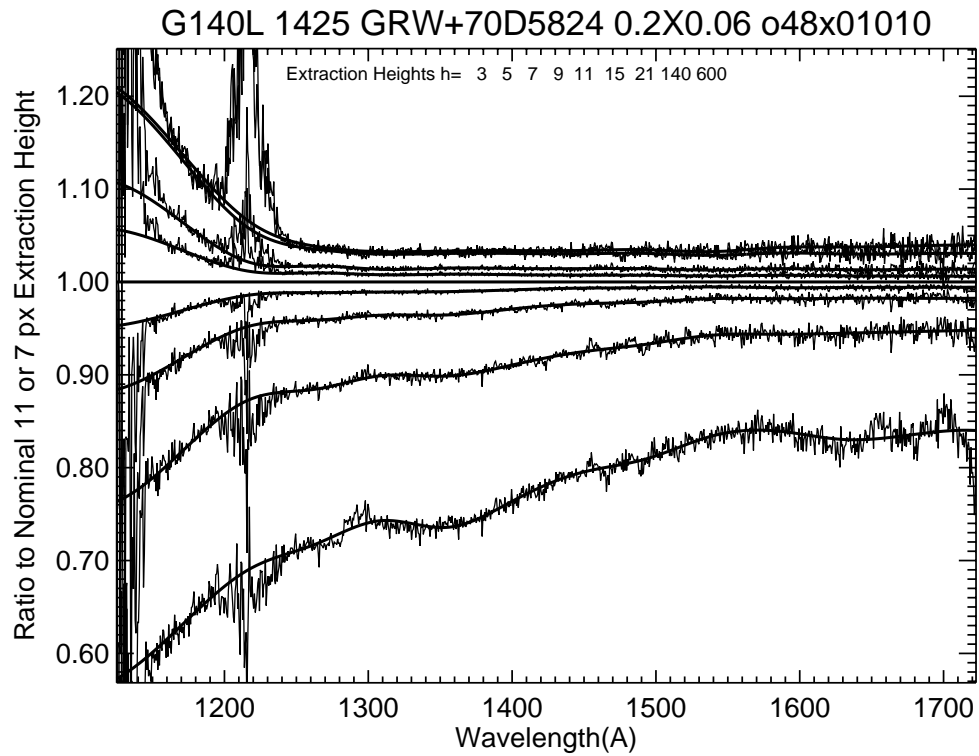


**Figure 3:** As in Figure 2, except for G230L.

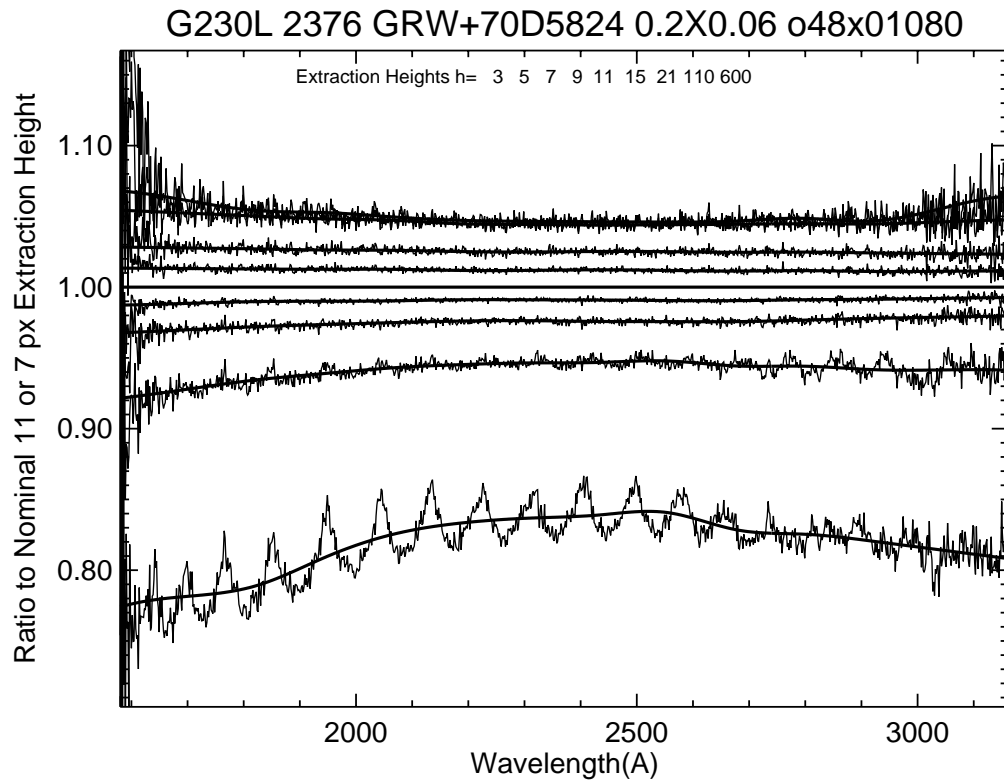


**Figure 4:**  $H(h)$  spline fits (heavy solid lines) and nodes (diamonds that often look like squares because of the overplotted error bars) for G140L and the 52x2 arcsec slit. Bars at each spline node are the  $1-\sigma$  scatter among the values of the spline fits for the multiple observations. Only the  $h=3$  extraction height has poor photometry with error bars greatly exceeding the size of the plotted symbols. A dashed line connects the largest  $h=600$  extraction. The dotted line connects the second largest extraction height, which contains ~99% of the signal and is occasionally a more robust estimate of the total signal. Results for some medium dispersion settings with the 52x2 arcsec slit are overplotted as open triangles.

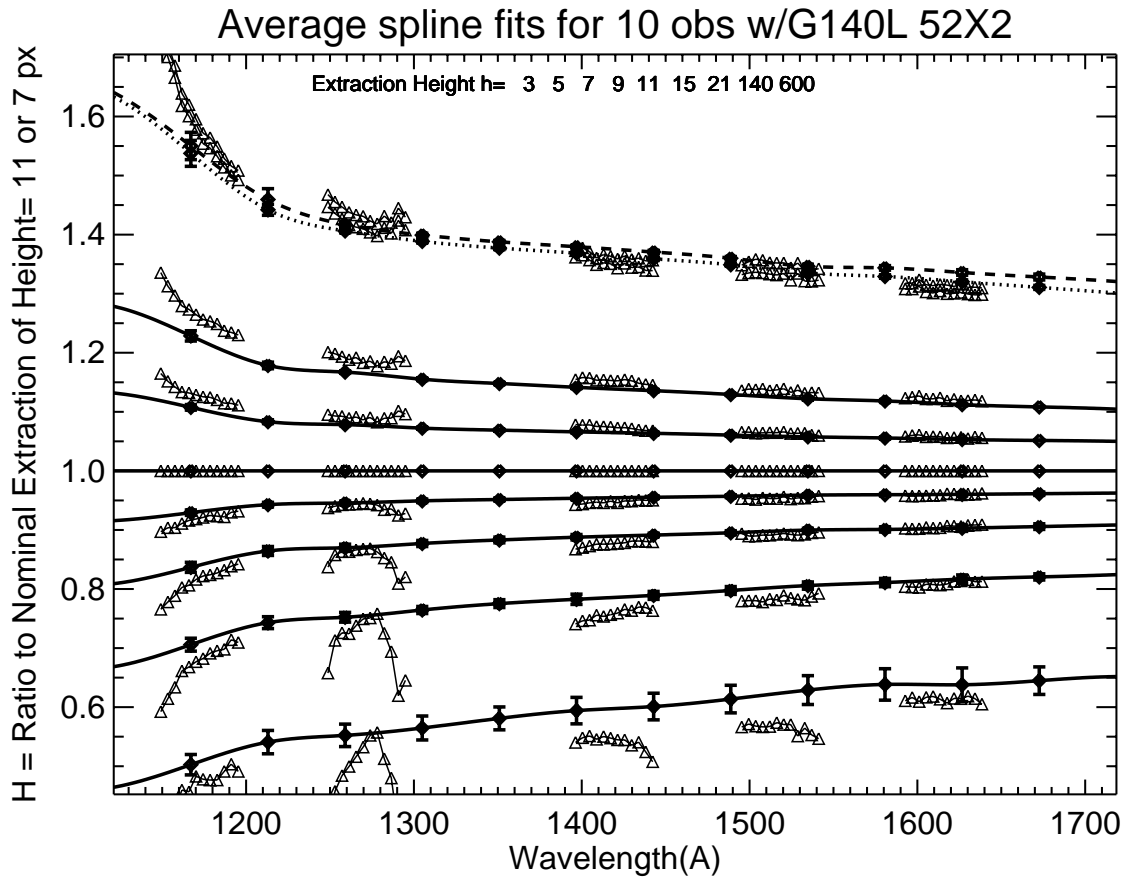


**Figure 5:** See Figure 4 caption, except for G230L.

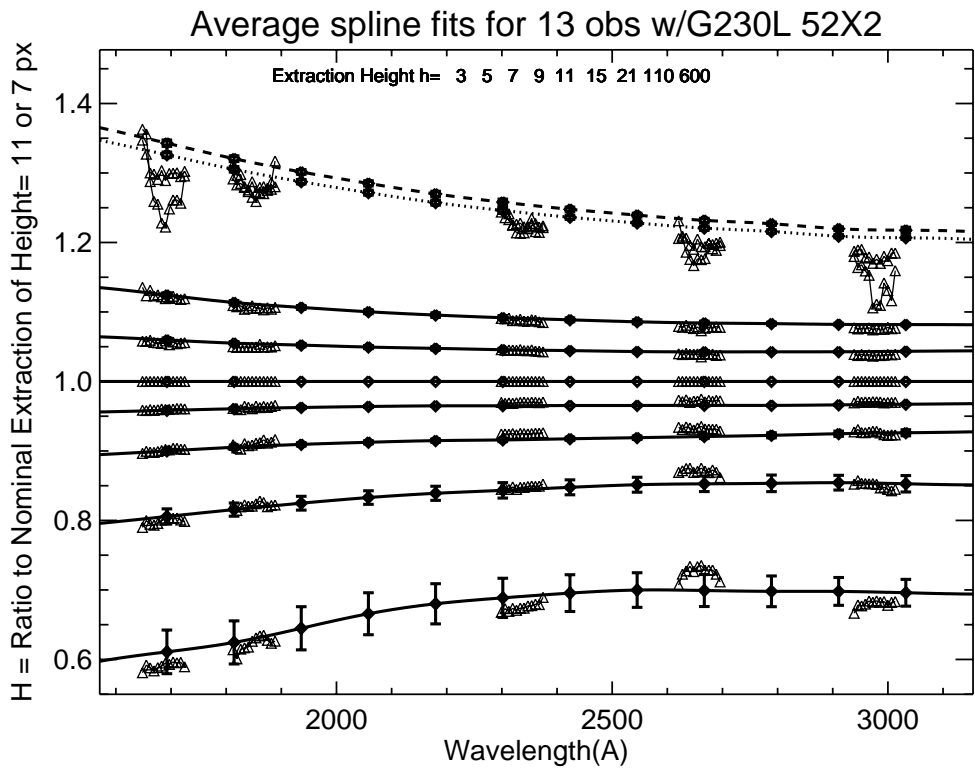


**Figure 6:** See Figure 4 caption, except for G230LB.

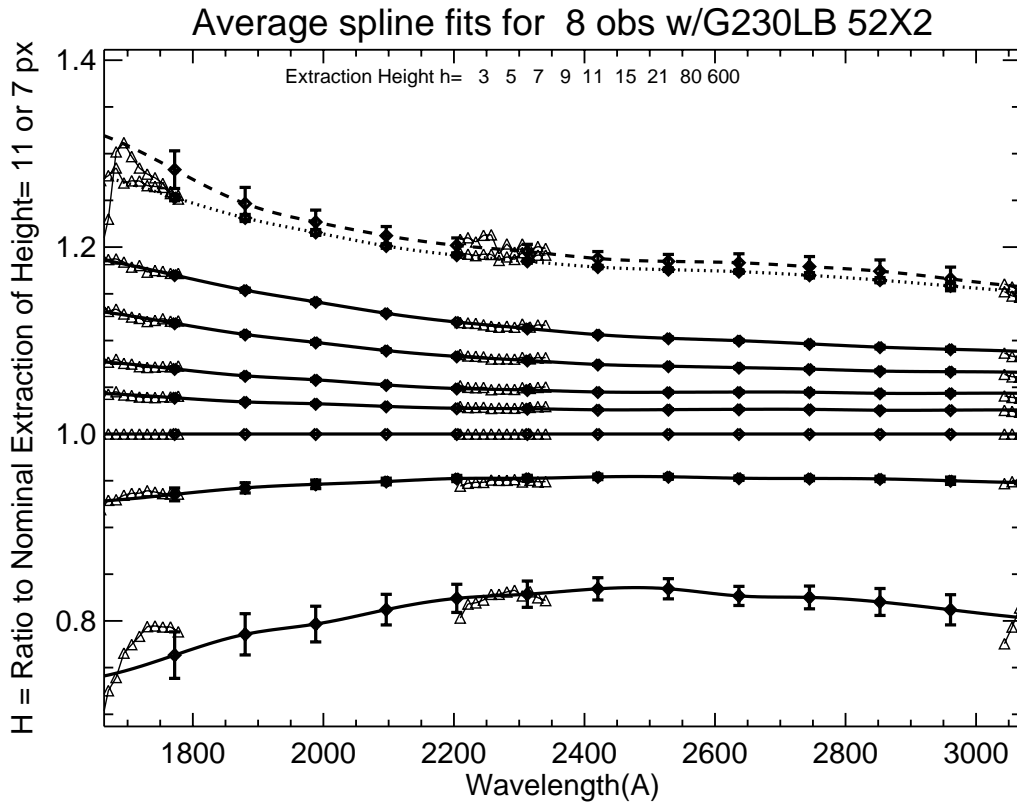


**Figure 7:** See Figure 4 caption, except for G430L.

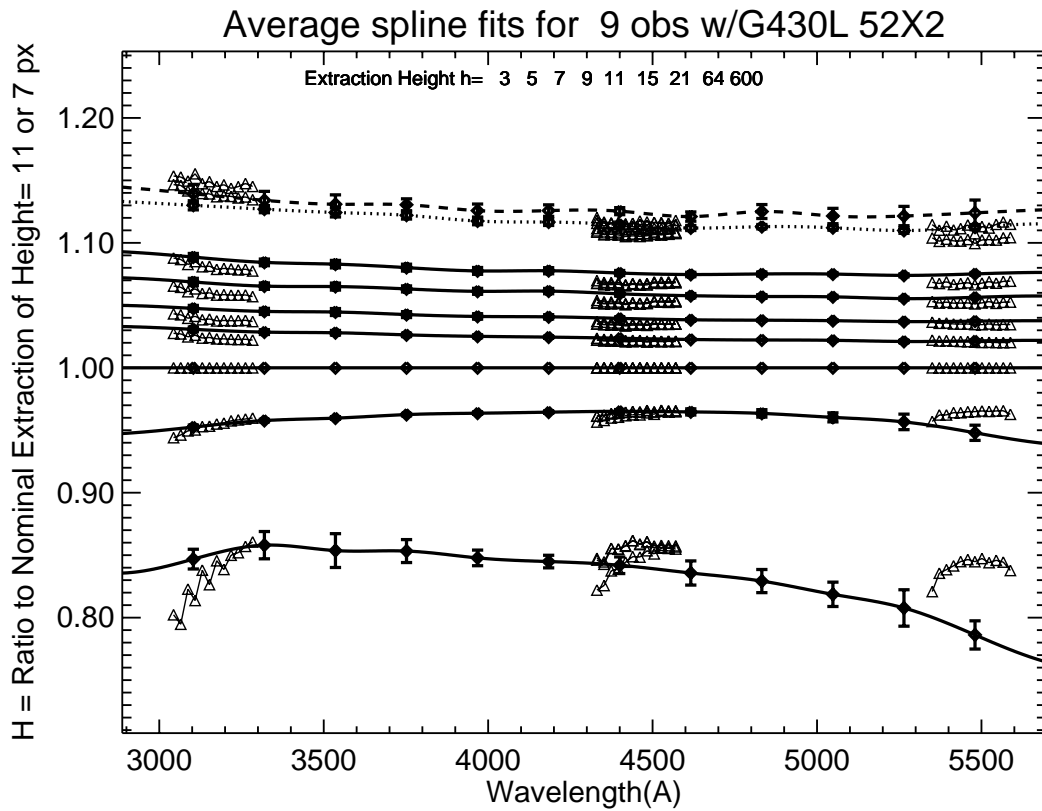


**Figure 8:** See Figure 4 caption, except for G750L.

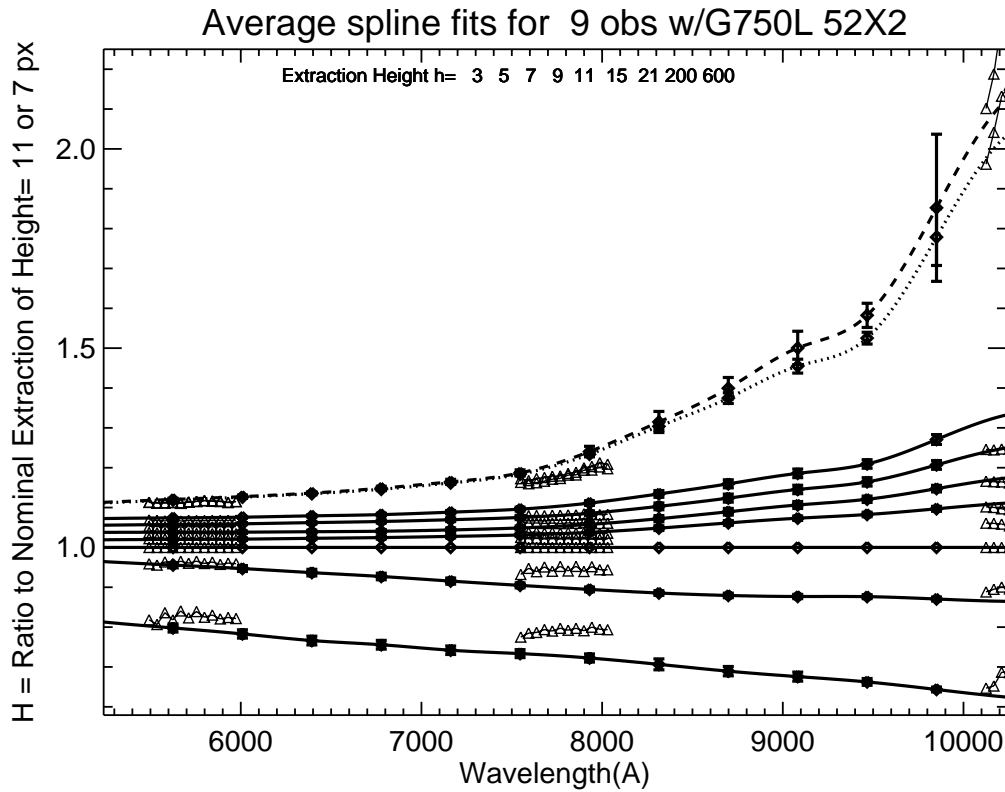


**Figure 9-30:** H(h) spline fits for many commonly used entrance apertures per the entries in Table 2. Only one observation is available, and no rms scatter can be shown.

**Figure 9:**

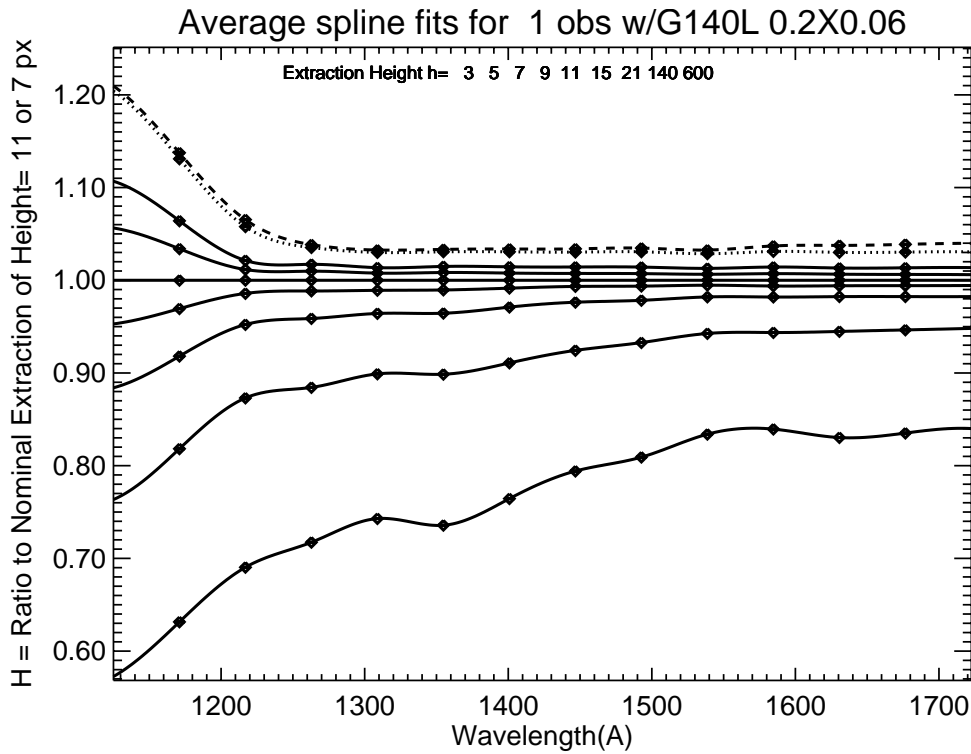


**Figure 10:** (see caption for Figure 9)

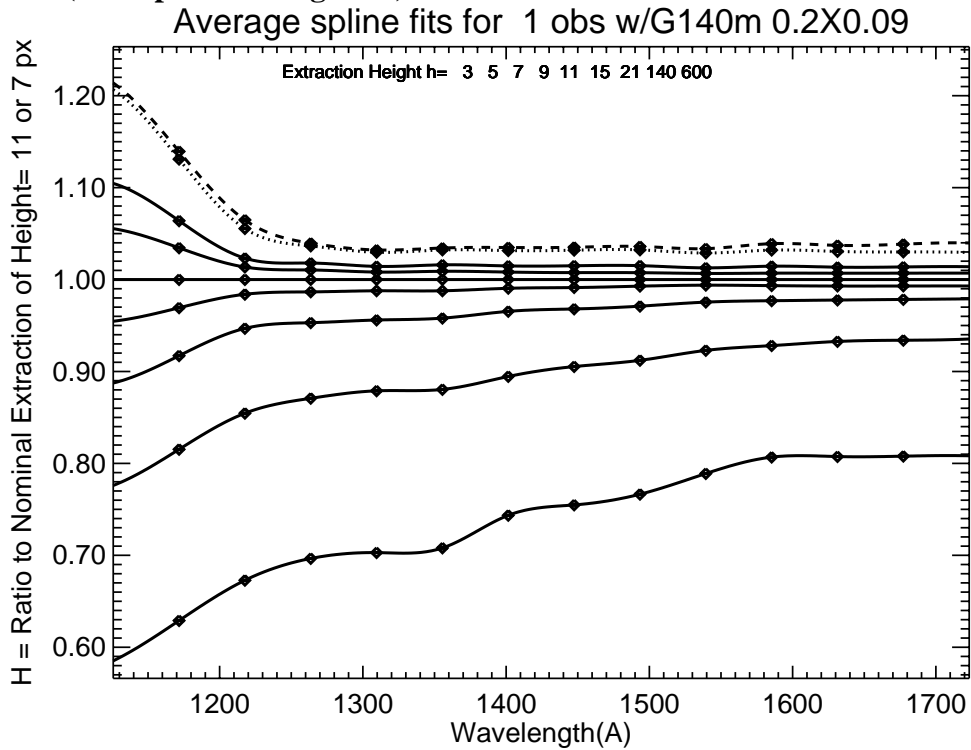


**Figure 11:** (see caption for Figure 9)

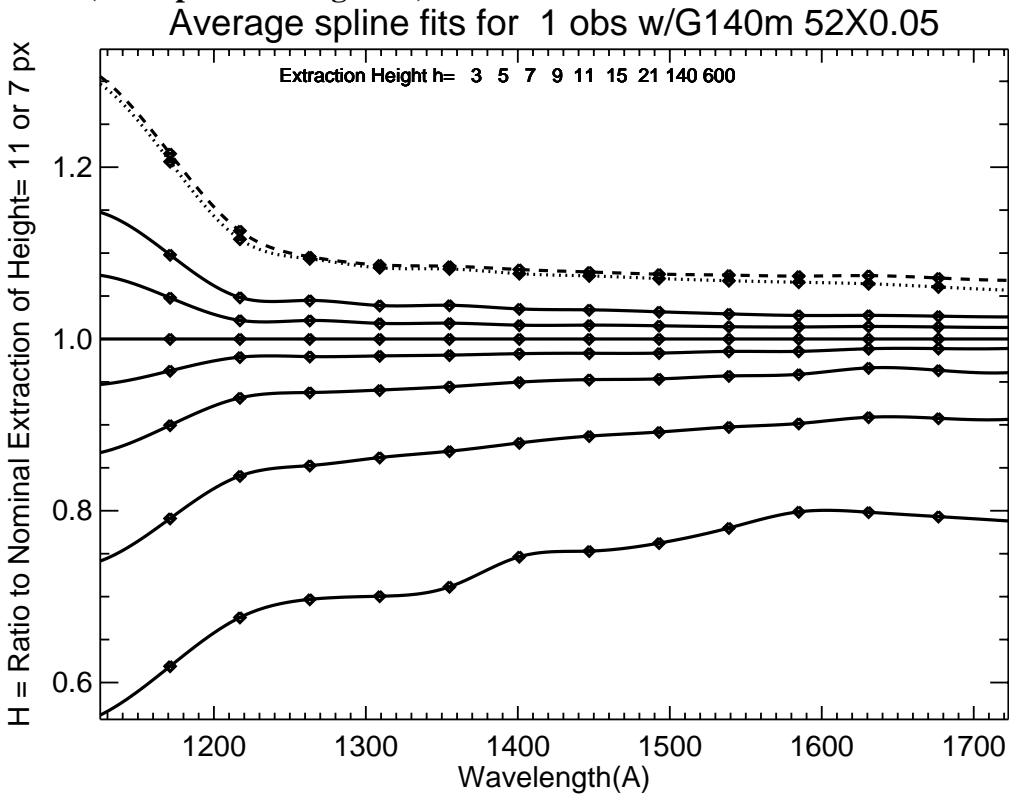


**Figure 12:** (see caption for Figure 9)

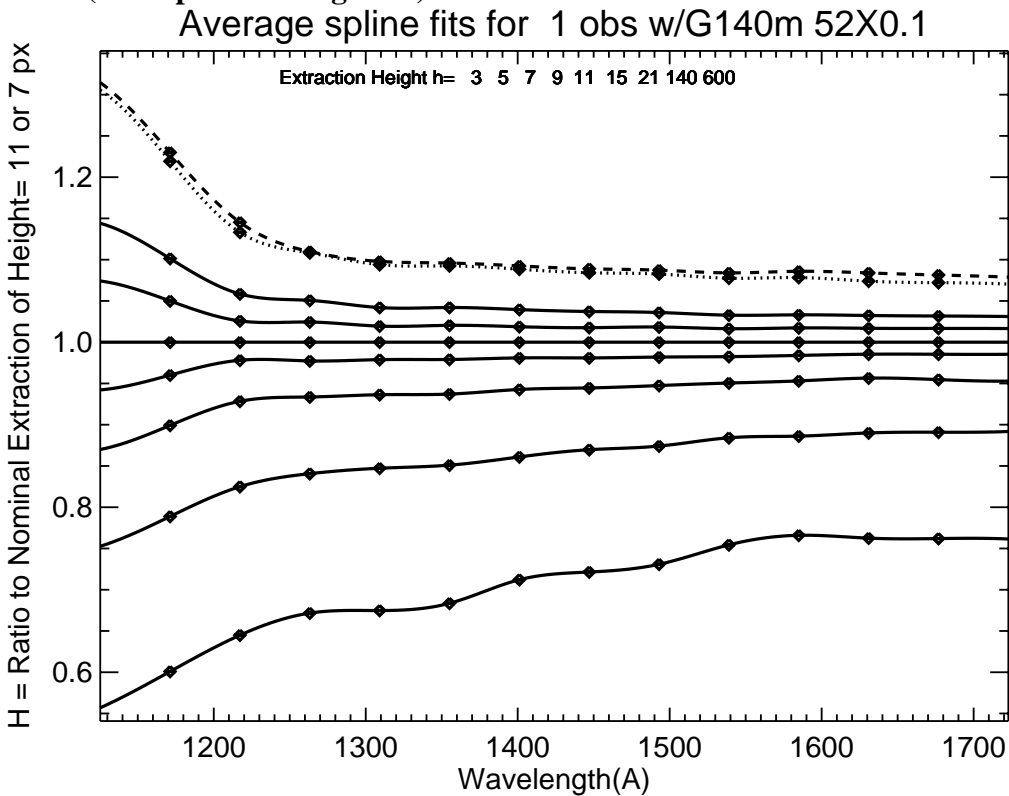


**Figure 13:** (see caption for Figure 9)

Average spline fits for 1 obs w/G140m 52X0.2

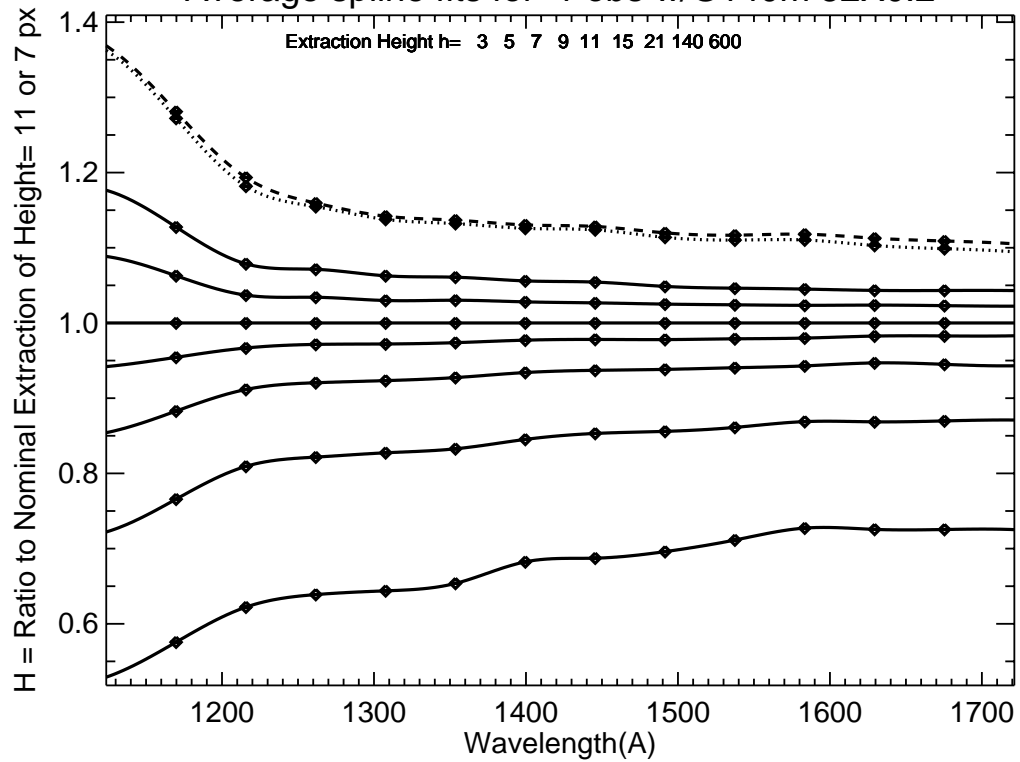


**Figure 14:** (see caption for Figure 9)

Average spline fits for 1 obs w/G140m 52X0.5

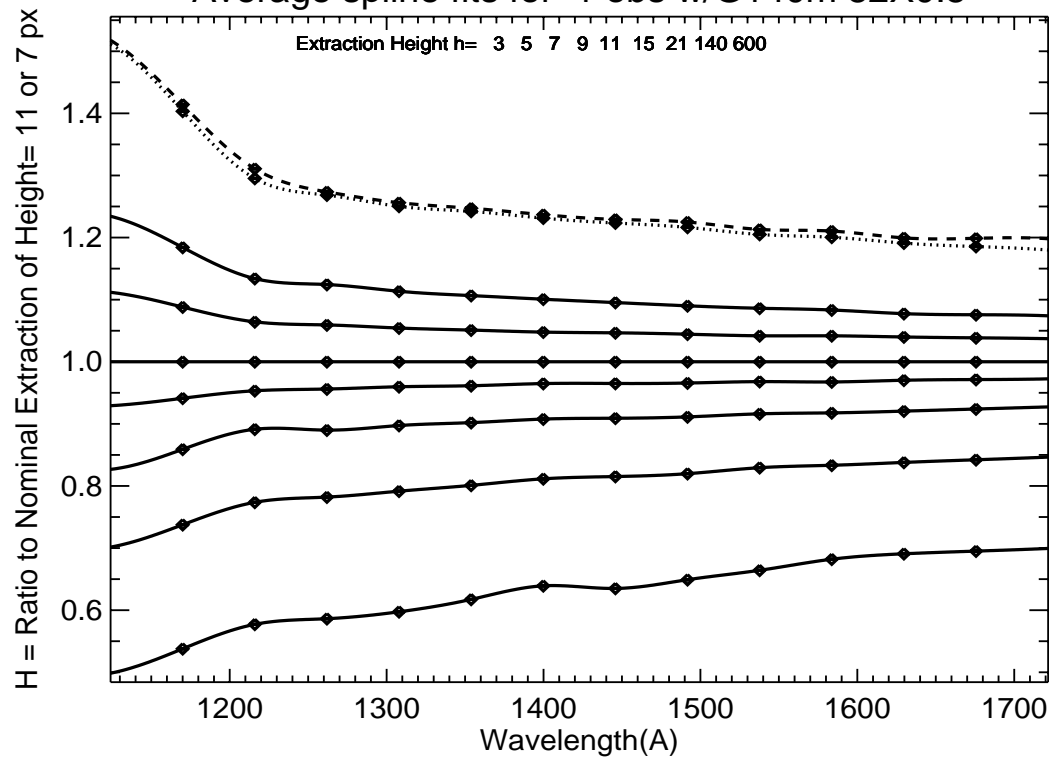


**Figure 15:** (see caption for Figure 9)

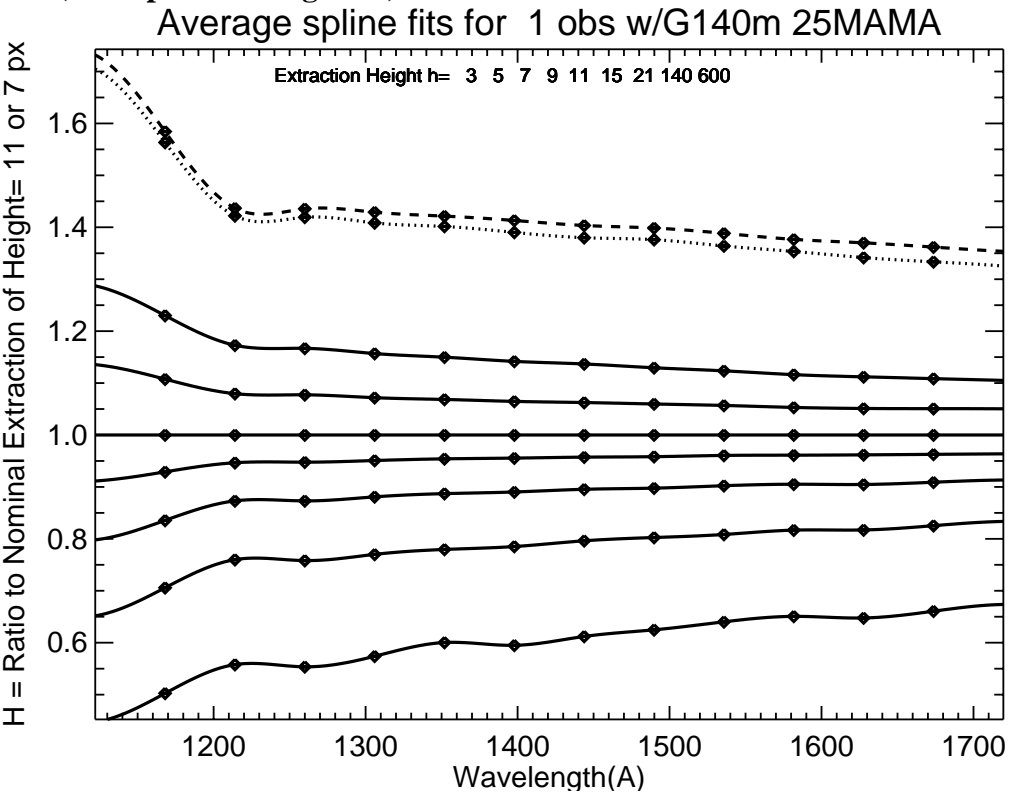


**Figure 16:** (see caption for Figure 9)

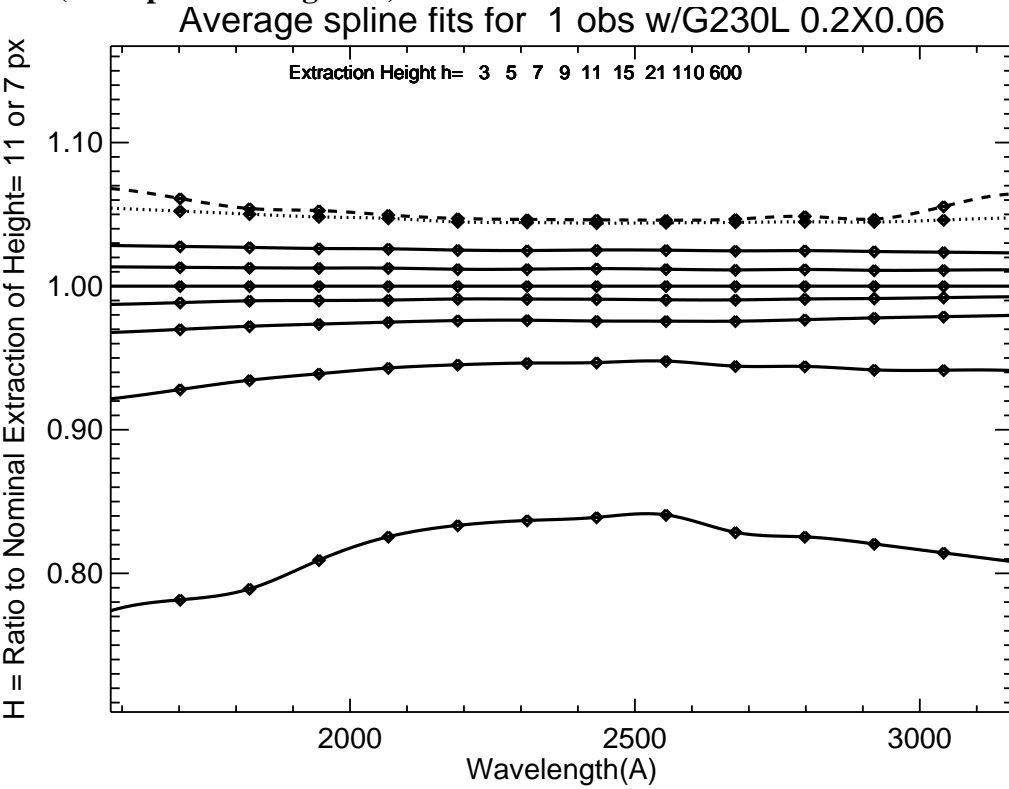


**Figure 17:** (see caption for Figure 9)

Average spline fits for 1 obs w/G230m 0.2X0.09

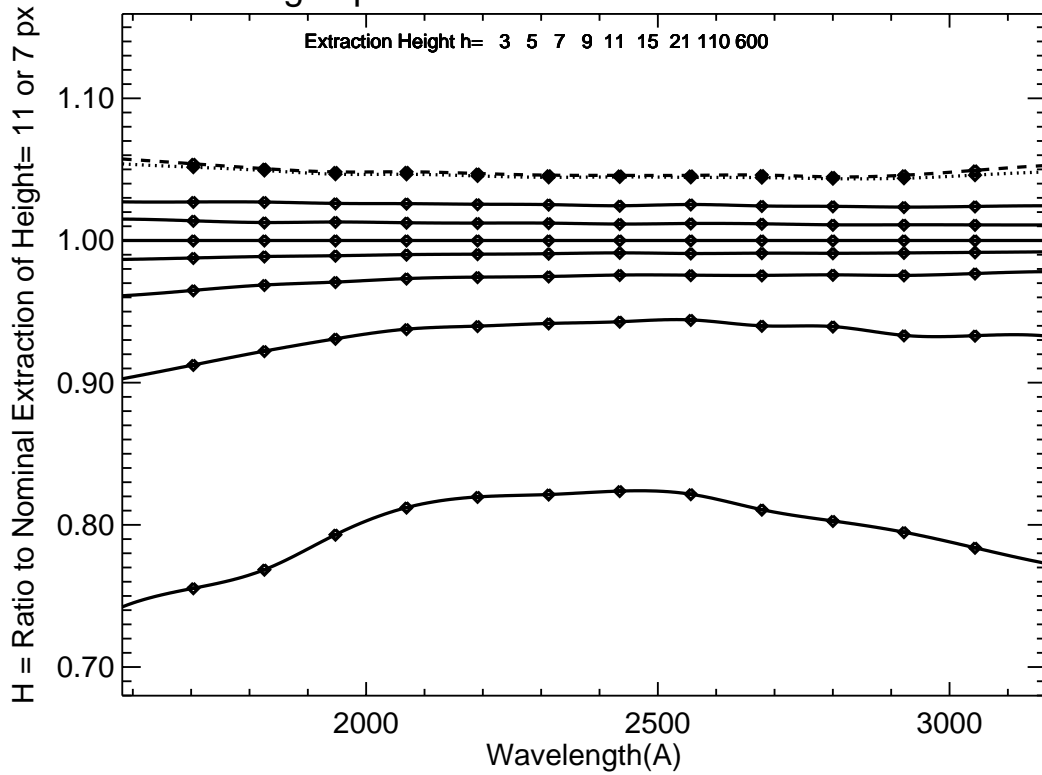


**Figure 18:** (see caption for Figure 9)

Average spline fits for 1 obs w/G230m 52X0.05

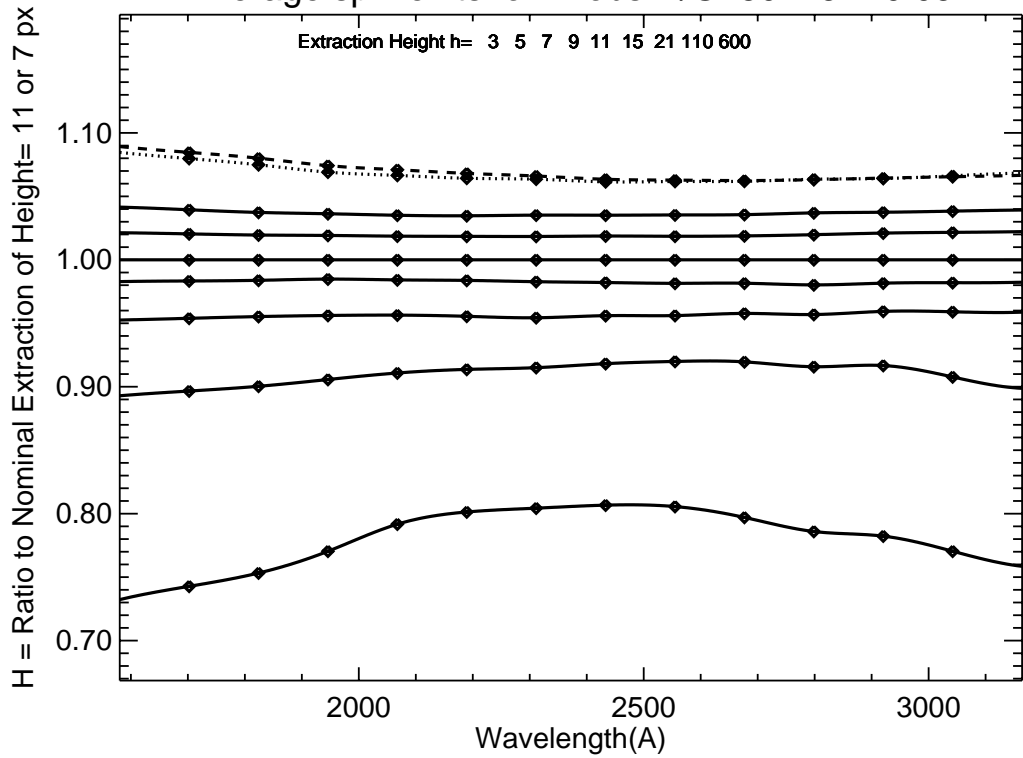


**Figure 19:** (see caption for Figure 9)

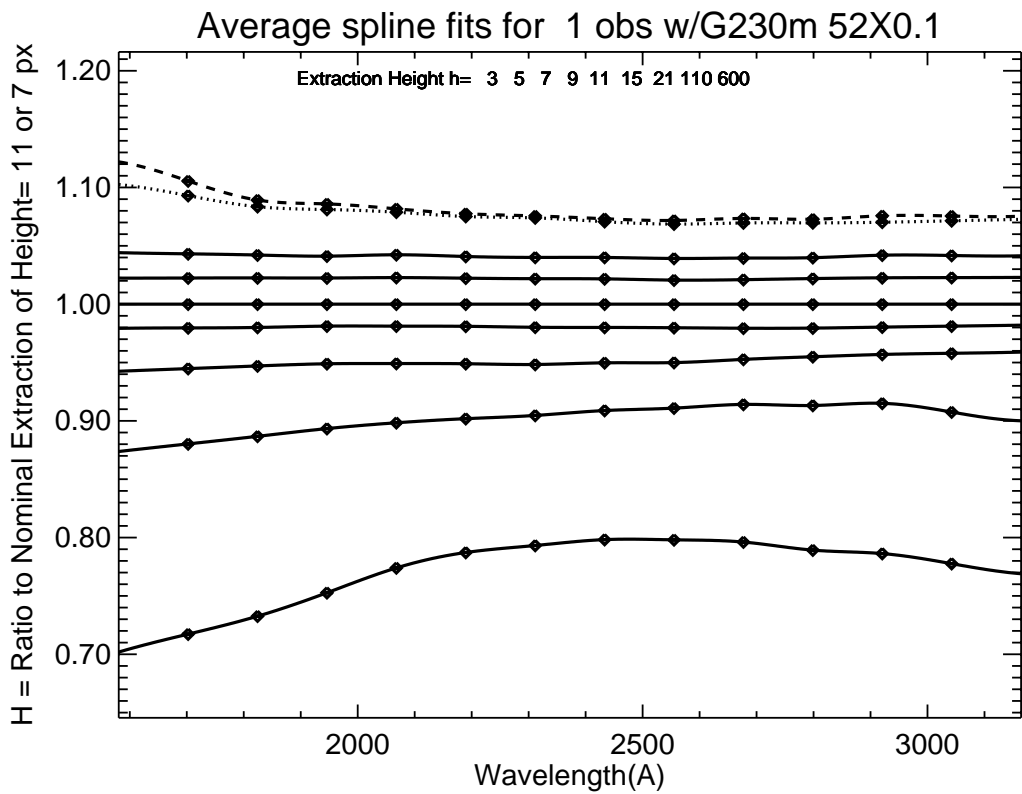


**Figure 20:** (see caption for Figure 9)

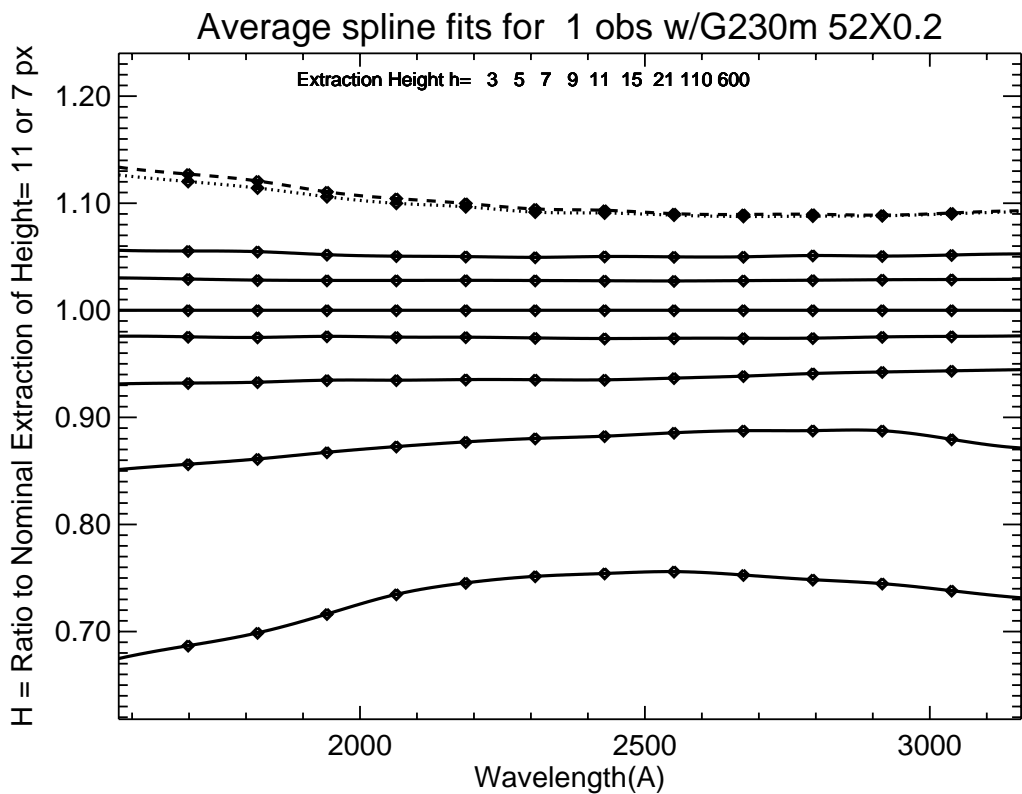


**Figure 21:** (see caption for Figure 9)  
 Average spline fits for 1 obs w/G230m 52X0.5

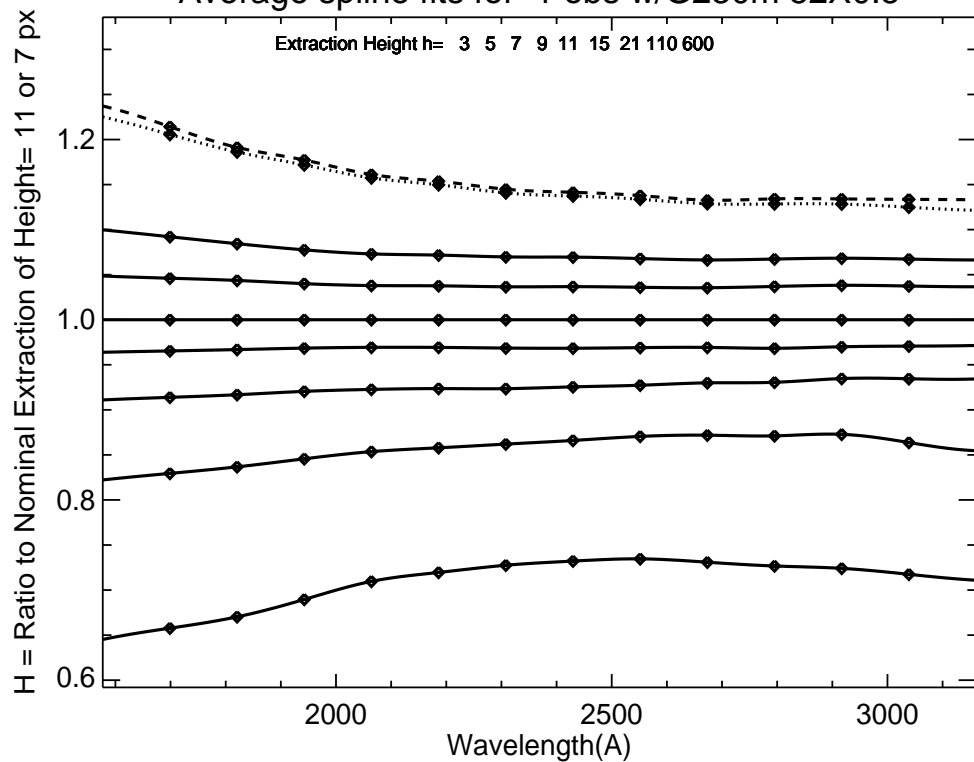


**Figure 22:** (see caption for Figure 9)  
 Average spline fits for 1 obs w/G230m 25MAMA

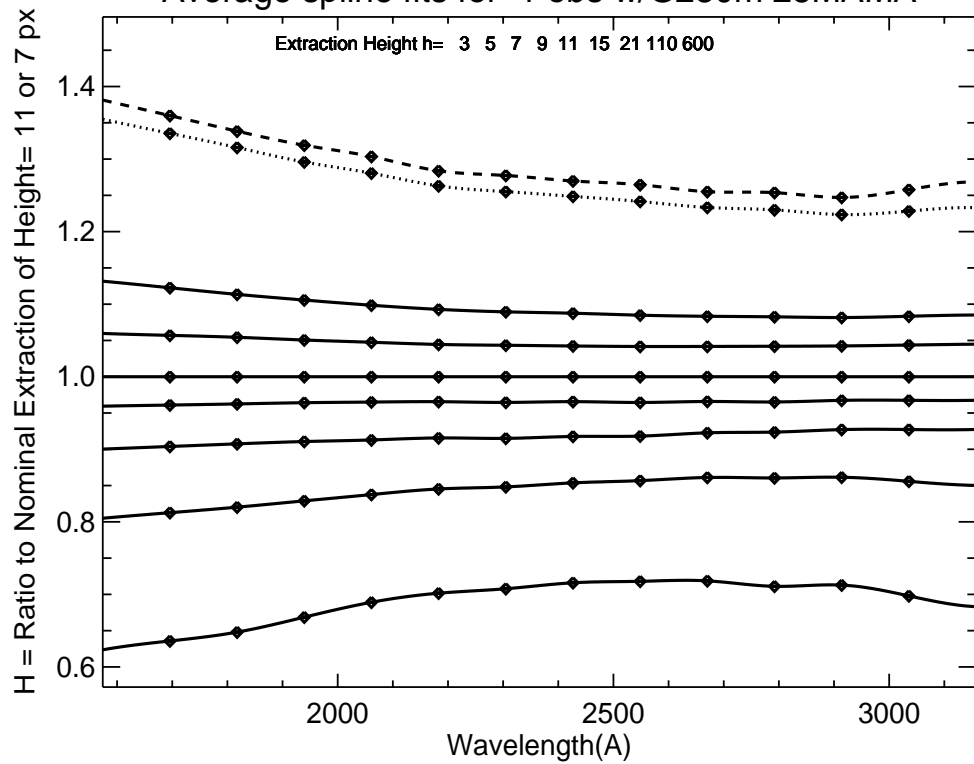


**Figure 23:** (see caption for Figure 9)

Average spline fits for 1 obs w/G430L 52X0.05

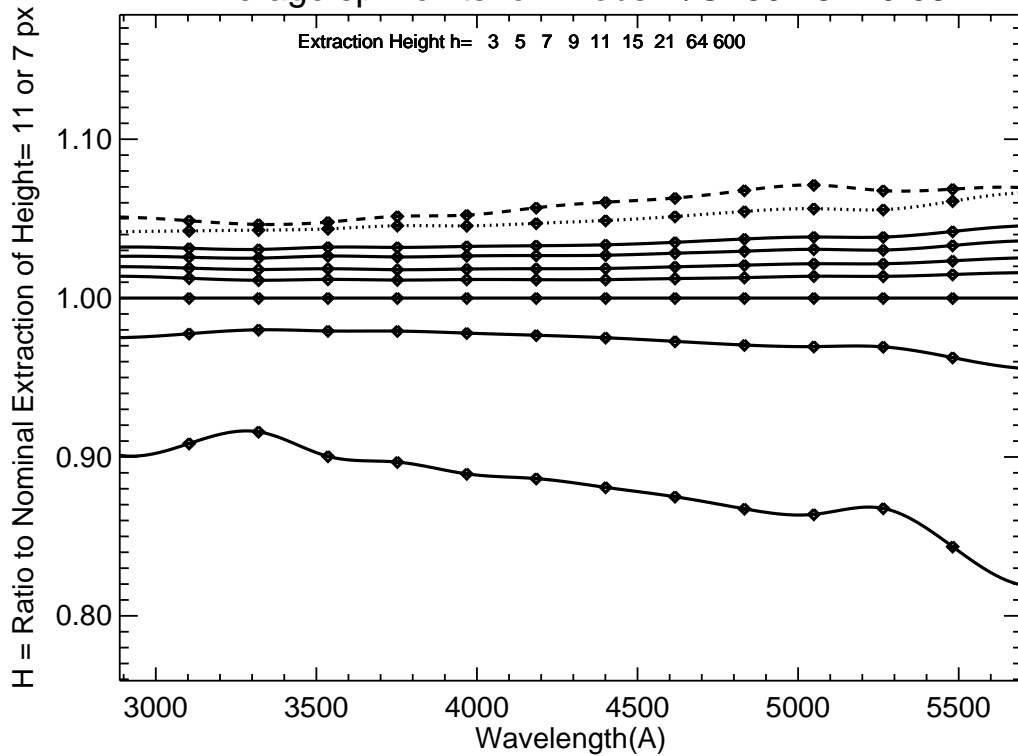


**Figure 24:** (see caption for Figure 9)

Average spline fits for 1 obs w/G430m 52X0.1

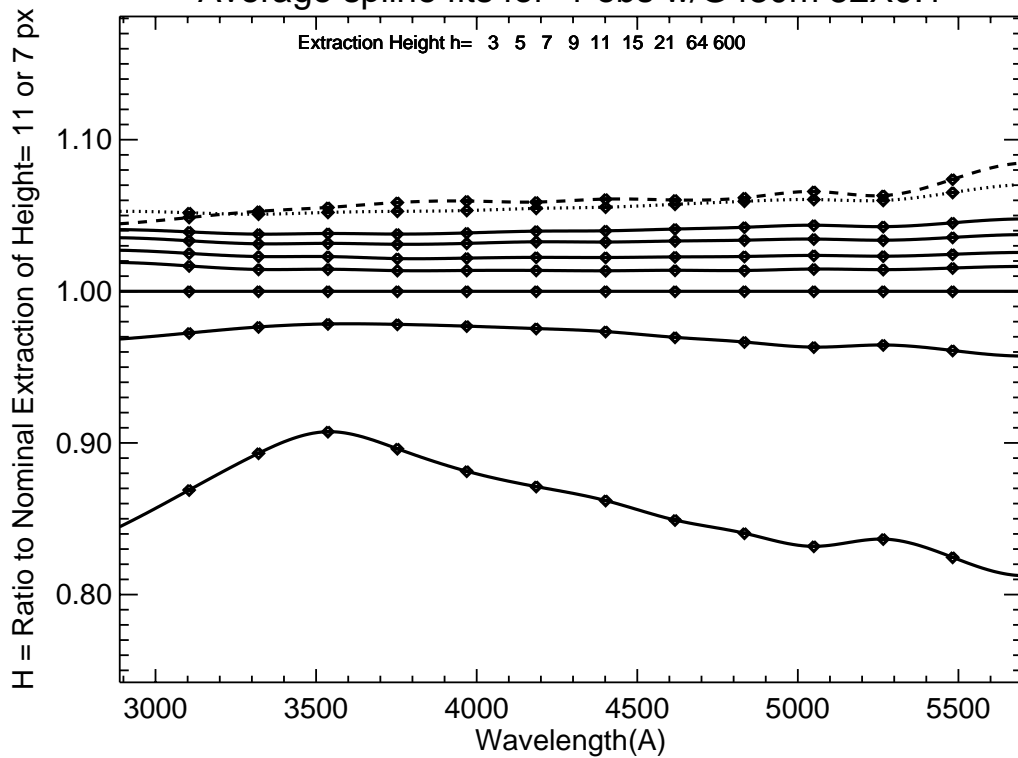


**Figure 25:** (see caption for Figure 9)

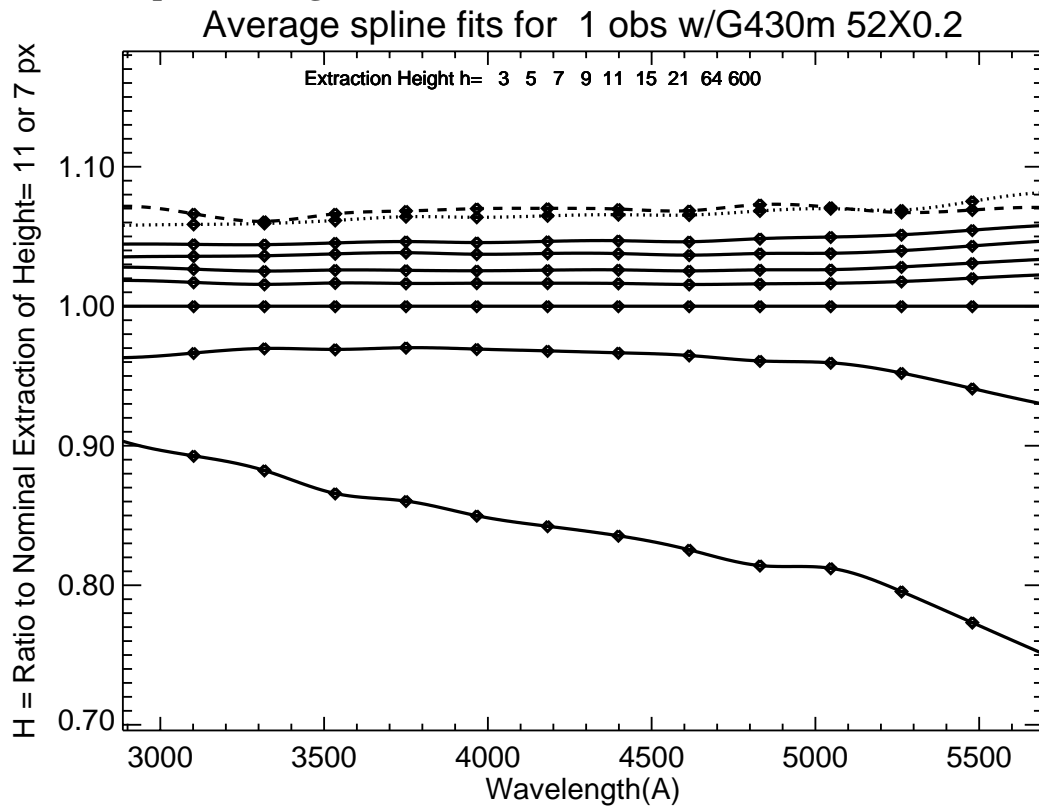


**Figure 26:** (see caption for Figure 9)

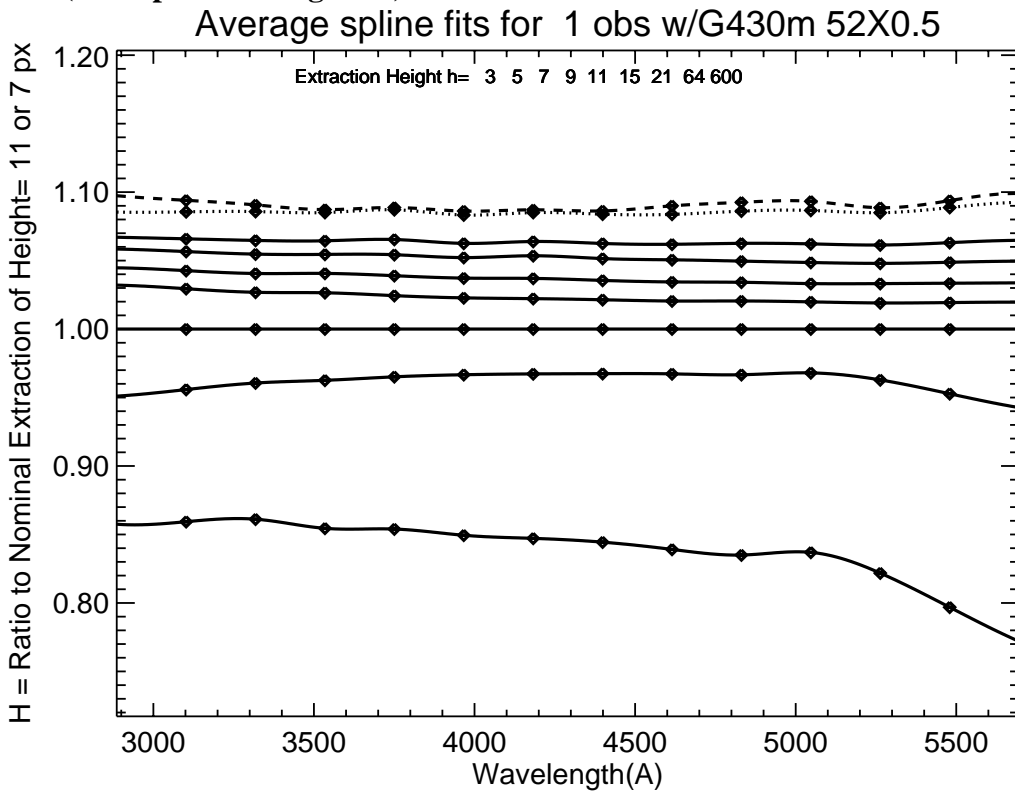


**Figure 27:** (see caption for Figure 9)

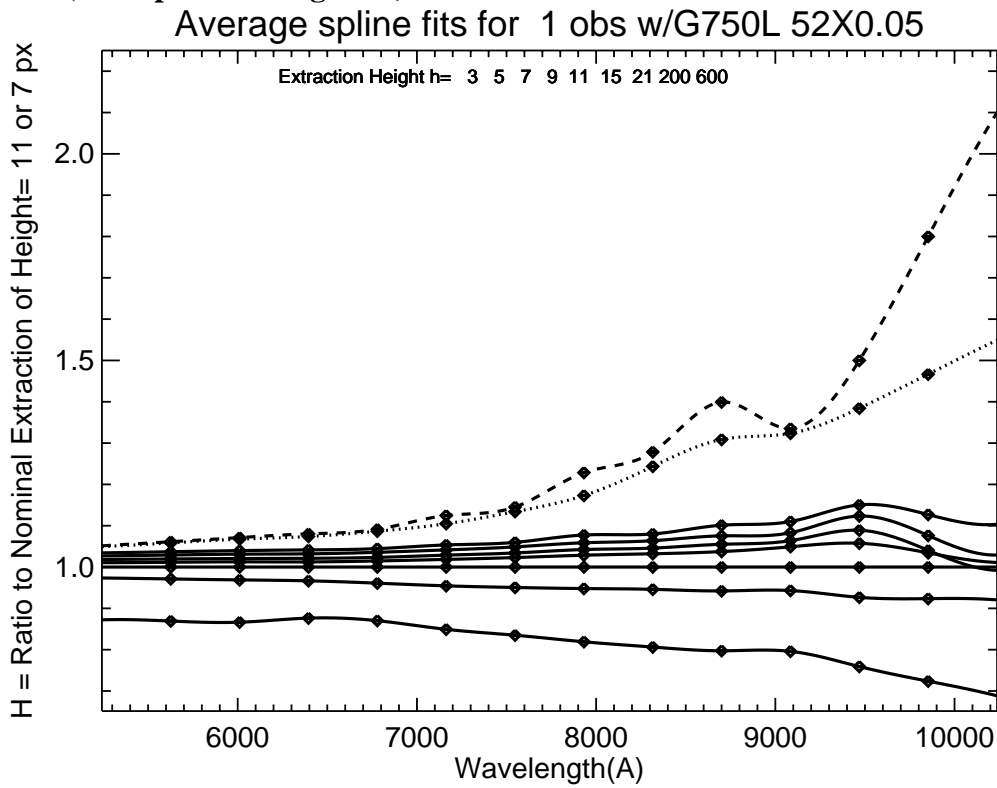


**Figure 28:** (see caption for Figure 9)

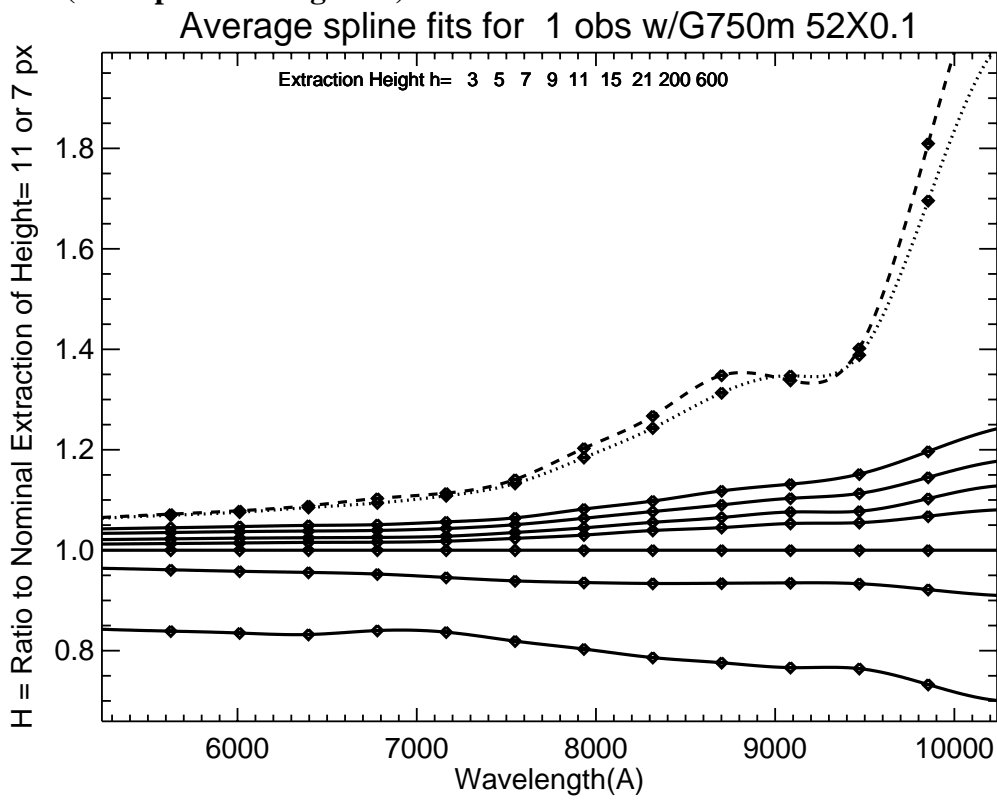


**Figure 29:** (see caption for Figure 9)

Average spline fits for 1 obs w/G750m 52X0.2

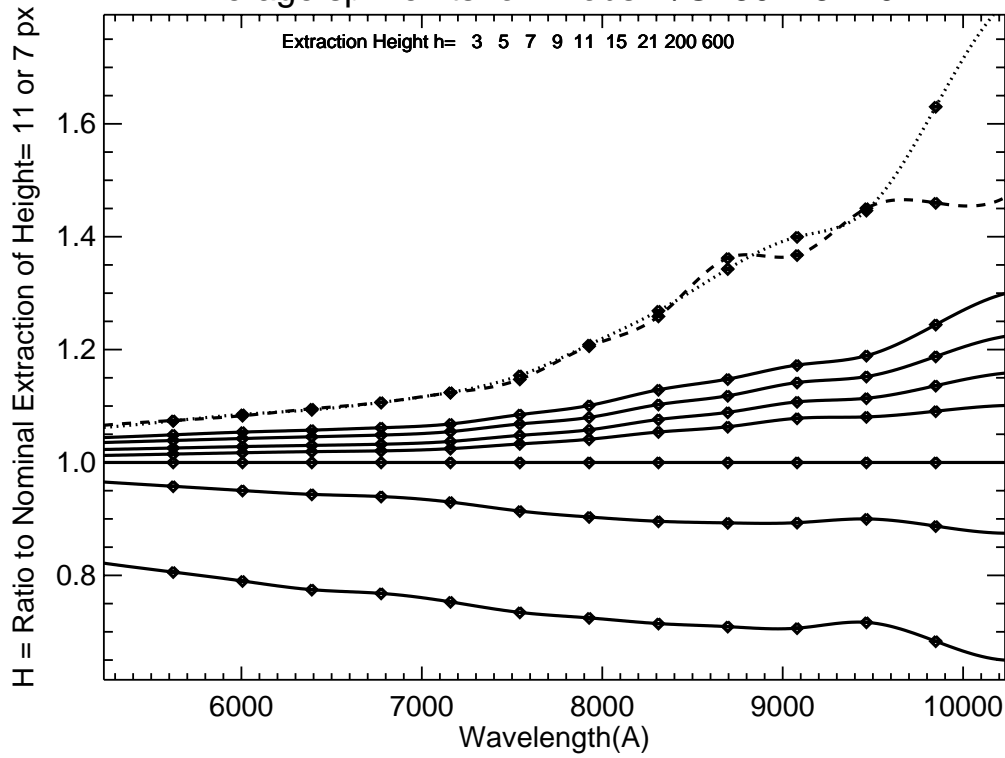


**Figure 30:** (see caption for Figure 9)

Average spline fits for 1 obs w/G750m 52X0.5

